atmosphere

MDPI

Article

Black Carbon Radiative Impacts on Surface Atmospheric Oxidants in China with WRF-Chem Simulation

Wei Dai [1,*], Keqiang Cheng [1], Xiangpeng Huang [2] and Mingjie Xie [1]

[1] Collaborative Innovation Center of Atmospheric Environment and Equipment Technology, Jiangsu Key Laboratory of Atmospheric Environment Monitoring and Pollution Control, School of Environmental Science and Engineering, Nanjing University of Information Science & Technology, Nanjing 210044, China

[2] Department of Environmental Science and Engineering, Shanghai Key Laboratory of Atmospheric Particle Pollution and Prevention, Fudan University, Shanghai 200438, China; huangxp@fudan.edu.cn

* Correspondence: daiweideemail@nuist.edu.cn

Abstract: Black carbon (BC) changes the radiative flux in the atmosphere by absorbing solar radiation, influencing photochemistry in the troposphere. To evaluate the seasonal direct radiative effects (DREs) of BC and its influence on surface atmospheric oxidants in China, the WRF-Chem model was utilized in this study. The simulation results suggested that the average annual mean values of the clear-sky DREs of BC at the top of the atmosphere, in the atmosphere and at the surface over China are +2.61, +6.27 and −3.66 W m^{-2}, respectively. Corresponding to the seasonal variations of BC concentrations, the relative changes of the mean surface photolysis rates (J[O1D], J[NO_2] and J[HCHO]) in the four seasons range between −3.47% and −6.18% after turning off the BC absorption, which further leads to relative changes from −4.27% to −6.82%, −2.14% to −4.40% and −0.47% to −2.73% in hydroxyl (OH) radicals, hydroperoxyl (HO_2) radicals and ozone (O_3), respectively. However, different from the relative changes, the absolute changes in OH and HO_2 radicals and O_3 after turning off BC absorption show discrepancies among the different seasons. In the North China Plain (NCP) region, O_3 concentration decreases by 1.79 ppb in the summer, which is higher than the magnitudes of 0.24–0.88 ppb in the other seasons. In southern China, the concentrations of OH and HO_2 radicals reach the maximum decreases in the spring and autumn, followed by those in the summer and winter, which is due to the enhancement of solar radiation and the summer monsoon. Thus, BC inhibits the formation of atmospheric oxidants, which further weakens the atmospheric oxidative capacity.

Keywords: black carbon; direct radiative effects; photolysis rate; ozone

Citation: Dai, W.; Cheng, K.; Huang, X.; Xie, M. Black Carbon Radiative Impacts on Surface Atmospheric Oxidants in China with WRF-Chem Simulation. *Atmosphere* **2024**, *15*, 1255. https://doi.org/10.3390/atmos15101255

Academic Editor: Avelino Eduardo Saez

Received: 11 September 2024
Revised: 9 October 2024
Accepted: 18 October 2024
Published: 21 October 2024

1. Introduction

Black carbon (BC) is a light-absorbing component in particulate matter, which is primarily present in the $PM_{2.5}$ size fraction (particles smaller than 2.5 μm). The absorption of BC directly alters the solar radiation flux in the atmosphere, which is called the direct radiation effect (DRE) [1]. The DRE of BC has been estimated through model simulations, where the estimated global average DRE of BC reaches from 0.19 to 0.53 W m^{-2} [2–4]. However, the annual average DRE of BC at the top-of-atmosphere (TOA) ranges from 1.2 to 4.5 W m^{-2} over China, which is higher than the global average [5–8]. BC not only changes the radiation budget, but also impacts the near-surface photochemistry by altering the actinic flux. Photochemical reactions are driven by solar radiation, and the photolysis rates (J) can be calculated by the following formula:

$$J = \int F(\lambda)\ \sigma(\lambda, T)\ q(\lambda, T) d\lambda \quad (1)$$

where σ(λ, T) is the wavelength (λ) and temperature (T)-dependent absorption cross section of reactants, q(λ, T) is the quantum yield of the product and F(λ) is the solar actinic flux [9]. Photochemical reactions have a significant impact on the secondary pollutants in the planetary boundary layer. For example, tropospheric ozone (O_3) is formed from precursors such as nitrogen oxides (NO_x) and volatile organic compounds (VOCs) through a series of photochemical reactions. Notably, the photolysis rate of NO_2 (J[NO_2]) determines the formation rate of O_3 [10]. In addition, the abundance of tropospheric hydroxyl (OH) radicals also come from photochemical reactions. The OH radical is initiated by the photolysis of O_3 yielding an excited oxygen atom O^1D (J[O^1D]), which subsequently reacts with H_2O. In polluted atmosphere, the photolysis of formaldehyde (HCHO) is also an essential source for OH radicals. The production rate of HCHO to OH radicals is an order of magnitude higher than that of O_3 [11,12].

A few studies have estimated the effects of aerosols on photolysis rates in the lower troposphere. In urban areas, the sulfate and dust increase the average photolysis rates at the surface by 2% to 17%, while BC reduces the photolysis rate by 10% [13]. Using a global model, Tie et al. [14] indicated that aerosols in East Asia reduce HO_x (OH and HO_2 radicals) abundance by 5% to 10% and cause changes in O_3 by −1% to −4%. Tian et al. [15] suggested that aerosols cause changes of −15% to 6% in the OH radical production and −3% to 1% in the O_3 concentration over eastern China. Meanwhile, BC reduces the actinic flux by 3.3%, resulting in a decrease of approximately 3% to 4% in the photolysis rates and a 0.7% to 1.2% reduction in surface O_3 over eastern China. The scattering of aerosols increases the photolysis rates by 10% to 18%, but the absorption BC (especially the internal mixture) effect reduces them by 6% to 11%, which has opposite effects at the ground [16]. Li et al. [17] suggested that BC decreases the photolysis rates of J[O^1D] and J[NO_2] by 10% to 30%, thereby reducing the surface O_3 by 5% to 20% during the haze pollution in the Houston area. In Europe, BC leads to a reduction in the photolysis rate of up to 30% in southern Europe, where BC emissions are high. However, in northern Europe, there is not such a significant decrease in the photolysis rate due to the low BC emissions [18]. In another study, it was found that BC decreased J[O^1D] by 15% to 25% in northern Europe in August [19]. Gao et al. [20] demonstrated that O_3 in the North China Plain (NCP) is more sensitive to BC compared to other scattering aerosols, when BC reduction exceeds 75%, the concentration of O_3 increases by more than 5 ppb. In the Beijing–Tianjin–Hebei (BTH) and the Yangtze River Delta (YRD) regions, the absorption of BC led to a reduction in the annual J[NO_2] (J[O^1D] by 14.90% (20.53%) and 13.71% (18.20%), respectively. In addition, the reduction in photolysis rates at noon was 2% to 3% higher than the daily average [21]. Previous studies have indicated that the reduction in J[O^1D] (J[NO_2]) caused by BC ranges from 11.4% to 17% (12.5% to 14%) in the BTH and YRD regions in China [22,23]. In the North China Plain (NCP), BC leads to a reduction of 2.0 ppb (7.8%) in the maximum daily 8-h average (MDA8) O_3 concentration in the daytime during a case study [23]. As a result, evaluating the impact of BC on radiative flux and its effects on surface atmospheric oxidants can contribute to our understanding of the role of BC in photochemistry.

So far, there has been limited research on the effect of BC on the photochemistry in the boundary layer in China. In this study, we evaluated the impact of BC absorption on solar radiation and further explored its influence on atmospheric oxidants (HO_x radicals and O_3). The Weather Research and Forecasting model coupled with Chemistry (WRF-Chem) was utilized to simulate the seasonal variations in BC spatial distributions over China in 2015, and a sensitivity experiment was designed to assess the impact of BC on the solar radiation flux and photolysis rates of HO_x radicals and O_3. The objective of this study is to provide an important reference for understanding the role of BC in photochemistry.

2. Methods

2.1. Model Configuration

The WRF-Chem model version 3.9.1 was utilized, which conducts simulations over a domain that contains 210 × 160 grid cells in a 37-km horizontal resolution over China and

its adjacent regions (Figure 1) [24]. Additionally, the model incorporates 32 vertical layers extending from ground level to the uppermost pressure level (50 hPa). This study employs the Model for Ozone and Related Chemical Tracers (MOZART) for the gas-phase reaction scheme [25]. As for aerosol chemistry, the Model for Simulating Aerosol Interactions and Chemistry (MOSAIC) was adopted for the aerosol parameterization [26]. Recent studies have suggested that organic carbon (OC) also exhibits light-absorbing effects, but the contribution of OC absorption to the absorbing aerosol optical depth (AAOD) at 440 nm is less than 25% and has a certain degree of uncertainty [27,28]. Therefore, the imaginary parts of the refractive indexes of OC and BC were set to 0.0 and 0.71, respectively [29]. More details of the model parameterization settings are available in Table 1. To improve the accuracy of meteorological variables in model simulations, the simulated wind, temperature and water vapor were adjusted towards the fifth generation European Centre for Medium-Range Weather Forecasts (ECMWFs) reanalysis (ERA5) data by using a 6-h nudging time scale. The nudging coefficient was set to 1×10^{-4} s^{-1} for all variables.

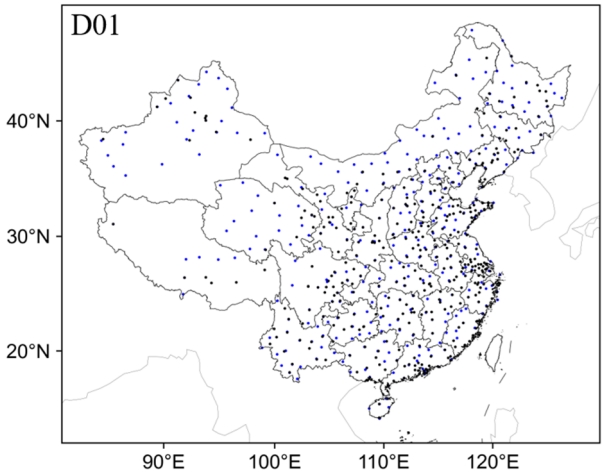

Figure 1. The domain of Weather Research and Forecasting model coupled with Chemistry (WRF-Chem) and the surface meteorological (blue dots) and environmental (black dots) observation stations in China.

Table 1. WRF-Chem model configurations.

Item	Settings	Reference
Microphysics scheme	Morrison double moment	[30]
Cumulus option	Grell 3D ensemble scheme	[31]
Longwave scheme	RRTMG scheme	[32]
Shortwave scheme	RRTMG scheme	[32]
Land surface scheme	Noah land surface model	[33]
PBL scheme	YSU scheme	[34]

The meteorological initial and boundary conditions were provided by the ERA5 data with a spatial resolution of 0.25° × 0.25° [35]. Anthropogenic emissions were obtained from the multi-resolution Emission Inventory for China (MEIC, version 1.4) and MIX for surrounding areas (http://meicmodel.org/, accessed on 12 June 2024), which is developed by Tsinghua University [36–38]. Biogenic emissions were generated using the Model of Emissions of Gases and Aerosols from Nature (MEGAN) [39]. The real-time biomass burning emissions were calculated from the Global Fire Emission Database version 4 with small fires (GFED4s) [40,41]. The chemistry initial and boundary conditions adopted the results from the Community Atmosphere Model with Chemistry (CAM-chem) (https://www.acom.ucar.edu/cam-chem/cam-chem.shtml, accessed on 12 June 2024) [42,43].

2.2. Observation Data

The meteorological and chemical observation data were used to verify model performance. Surface meteorological observations with a temporal resolution of 3 h were provided by the National Climatic Data Center of National Oceanic and Atmospheric Administration (NOAA, https://www.ncei.noaa.gov/maps/hourly/, accessed on 12 June 2024). The specific meteorological elements were 2-m temperature (T_{2m}), 2-m relative humidity (RH_{2m}) and 10-m wind speed (WS_{10m}). The hourly $PM_{2.5}$ concentration data were obtained from the China National Environmental Monitoring Centre (CNEMC, https://air.cnemc.cn:18007/, accessed on 12 June 2024). Ground-based aerosol optical depth (AOD) observations and AAOD measurements at Xiang He station (116.96° E, 39.75° N) were derived from the Aerosol Robotic Network (AERONET) version 3 level 2.0 products [44].

2.3. Experimental Designs

The simulation was conducted from 27 December 2014 to 31 January 2015, from 27 March to 30 April 2015, from 26 June to 31 July 2015 and from 26 September to 31 October 2015, respectively. The spin-up time of the model is 5 days prior to each simulation period, and the results during the spin-up time are not included in the analysis. Following previous studies, we used the entire months of January, April, July and October to represent winter, spring, summer and autumn, respectively [45–48]. In order to explore the impact of BC on clear-sky shortwave radiation flux and photolysis rates, the following two experiments have been carried out: (1) BASE—the baseline in which the absorption of BC is included in the calculation of aerosol optical properties and (2) NOBC—the same case as BASE, but with the absorption of BC turned off (the imaginary part of the refractive index of BC was set to 0). For the BASE case, the model default value of 0.71 was adopted for the imaginary part of the refractive index of BC. Following Yang et al. [49], the impact of BC absorption on the pollutants was analyzed by calculating the difference between BASE and NOBC simulations (i.e., BASE minus NOBC). When the difference between BASE and NOBC simulations is negative, it implies that BC has an inhibitory effect on pollutants, and when it is positive, it has a promoting effect on pollutants.

3. Results

3.1. Model Evaluation

When comparing the simulation results with the observed data, we interpolated the simulated data to the latitude and longitude of the observation site. The model performance was verified using the surface meteorological observations in the four seasons (Figure 2). The seasonal and annual average statistical metrics, including the correlation coefficient (R), normalized mean bias (NMB) and root mean square error (RMSE) for the different variables are listed in Table 2. The simulated T_{2m} and RH_{2m}, by the WRF-Chem model, exhibit a good agreement with the observations, with the R values reaching 0.92 to 0.97 and 0.80 to 0.95, respectively, in the four seasons. In the spring, the RMSE values for T_{2m} and RH_{2m} are 3.29 and 12.20 higher than that of the other seasons, suggesting that the model has slightly greater errors for T_{2m} and RH_{2m} in the spring than in the other seasons. The R value for WS_{10m} ranges from 0.56 to 0.73 in the different seasons, which are lower than those for T_{2m} and RH_{2m}. The seasonal NMB of WS_{10m} ranges from 28.5% to 50.7%, showing a tendency of overestimation. This over-predicting tendency of the surface wind speed in the WRF/WRF-Chem model is consistent with the findings in previous studies, which is due to the poor surface friction simulation by the surface-layer parameterization scheme [50–52].

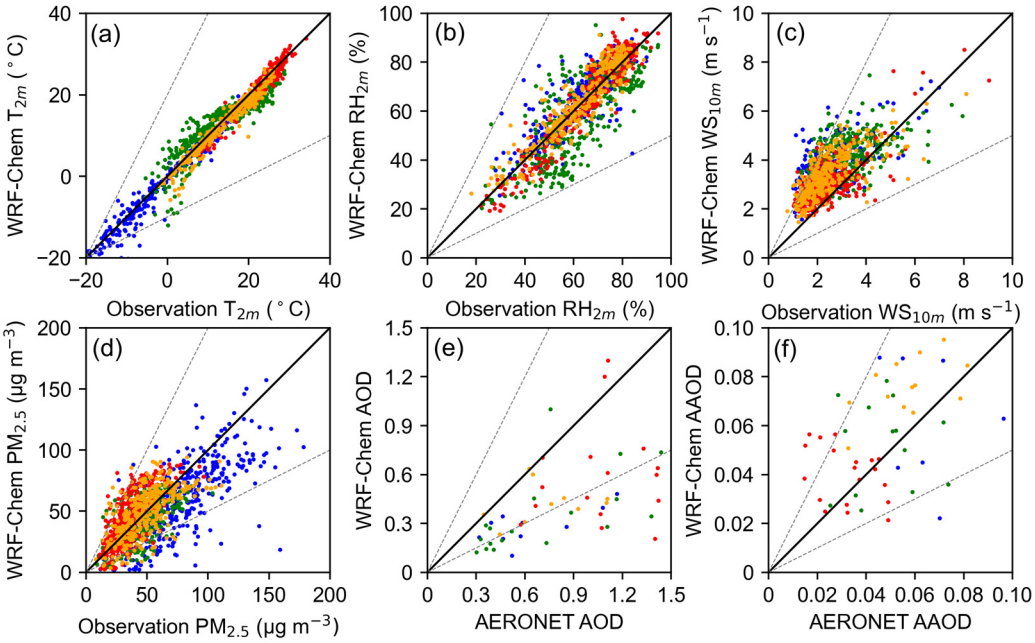

Figure 2. Scatter plots of simulated 2-m temperature (**a**), 2-m relative humidity (**b**), 10-m wind speed (**c**), $PM_{2.5}$ (**d**), aerosol optical depth (**e**) and absorption aerosol optical depth (**f**) versus surface observations in winter (blue dots), spring (green dots), summer (red dots) and autumn (yellow dots). The solid 1:1 lines and dashed 1:2 and 2:1 lines are shown for reference.

Table 2. Statistical metrics for evaluating performance of WRF-Chem model in simulating meteorological and chemical variables.

Variables	Statistic	Winter	Spring	Summer	Autumn	Annual
T_{2m} (°C)	*R*	0.96	0.92	0.97	0.97	0.96
	NMB	−11.2	2.2	−2.3	−6.0	−2.9
	RMSE	1.52	3.29	1.46	1.63	2.17
RH_{2m} (%)	*R*	0.85	0.80	0.95	0.93	0.86
	NMB	3.1	−7.3	0.46	2.22	0.3
	RMSE	7.54	12.20	5.61	5.73	8.21
WS_{10m} (m s^{-1})	*R*	0.67	0.56	0.70	0.72	0.67
	NMB	50.7	30.0	28.5	39.9	36.7
	RMSE	1.41	1.34	0.96	1.22	1.25
$PM_{2.5}$ (μg m^{-3})	*R*	0.72	0.61	0.73	0.66	0.70
	NMB	−23.1	−5.6	23.6	1.4	5.7
	RMSE	28.09	14.02	16.26	15.57	19.63
AOD	*R*					0.45
	NMB					−34.7
	RMSE					0.43
AAOD	*R*					0.48
	NMB					13.6
	RMSE					0.017

By comparing the WRF-Chem simulation with the observation from the CNEMC, it can be seen that the simulation results can generally capture the seasonal variation features of $PM_{2.5}$ concentration, with the *R* values reaching 0.61 to 0.73 in the four seasons, respectively. However, the RMSE and NMB values for $PM_{2.5}$ in the winter are 28.09 and −23.1%, respectively, indicating that the error of the simulated $PM_{2.5}$ in the winter is 28.09 μg m^{-3}, which is an underestimation of 23.1%. This is because the simulated WS_{10m} is about 50% higher than the observed values. By contrast, the model overestimates the $PM_{2.5}$ concentrations by 23.6% in the summer. Similar to previous studies, this bias is attributed to an overestimation in the secondary inorganic aerosols (i.e., nitrate and ammonium) [53–55]. To verify the optical properties of aerosols, the model simulations

were further compared with the AOD and AAOD at 550 nm from the AERONET [44]. It was found that the model underestimates the AOD by 34.7% but overestimates the AAOD by 13.6%. Overall, the WRF-Chem model can basically reproduce the temporal variations of meteorological and chemical variables.

3.2. Spatial Distribution and Direct Radiative Effect of Black Carbon

Figure 3 depicts the spatial distributions of the simulated seasonal mean surface BC concentrations in China. The BC concentrations are higher in densely populated and industrially developed areas, such as the NCP, the Yangtze River Delta (YRD) and the Sichuan Basin (SCB). The seasonal mean BC concentrations in China are 0.70, 0.28, 0.19 and 0.38 μg m^{-3} in the winter, spring, summer and autumn, respectively. In the winter, residential activities emit BC between 1.5 and 2 times more than those in the other seasons in China, leading to the highest BC concentrations [38]. In eastern China, cold, high pressure prevails in the winter, with the low boundary layer height and weak wind speed contributing to the accumulation of pollutants, while in the summer, under the control of the East Asian summer monsoon, the high boundary layer height and increased precipitation facilitating the diffusion and scavenging of pollutants [56–58]. Correspondingly, the AAOD values in the east part of China are higher than those in the west part because BC is the predominant light-absorbing aerosol. The seasonal mean AAOD in China reaches its highest value of 0.015 in the winter, followed by 0.011 in the spring and autumn, and its lowest value of 0.010 in the summer. In the summer, the AAOD is not significantly lower than the BC concentration in the other seasons, which is due to the higher humidity in the troposphere during the summer [59]. Liu et al. [28] have indicated that the annual and winter mean values of AAOD in China are 0.017 and 0.022, respectively, which are slightly higher than the simulation results in this study. In the summer, the highest AAOD of 0.026 is found in the NCP region, which is slightly lower than the previous simulation results of 0.03–0.05 in 2010 [8].

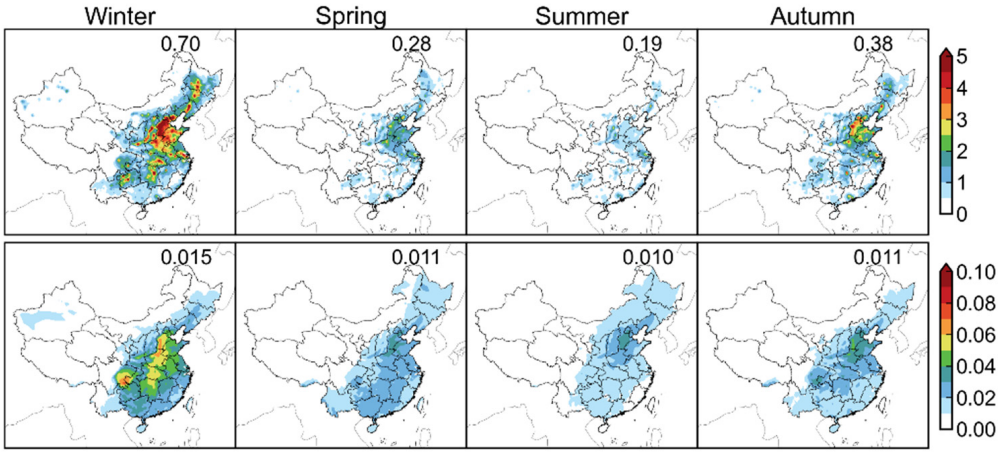

Figure 3. Spatial distributions of seasonal mean surface black carbon (BC) concentrations (**first row**) and AAOD at 550 nm (**second row**). Mean values averaged over China are shown in the upper right corner.

Figure 4 illustrates the spatial distributions of the seasonal clear-sky shortwave DREs of BC at the TOA, in the atmosphere and at the surface over China. The annual mean values of BC DREs at the TOA, in the atmosphere and at the surface are +2.61, +6.27 and −3.66 W m^{-2}, respectively. Previous studies have suggested that the annual mean BC DRE at the TOA ranges from +1.2 to +4.5 W m^{-2}, which is similar to the simulated results in this study [5–8]. The seasonal mean values of BC DREs at the TOA are +2.60, +3.03, +2.75 and +2.09 W m^{-2} in the winter, spring, summer and autumn, respectively. The values of BC DREs at TOA and ATM are 3.03 and 7.01 W m^{-2} in the spring, which are higher than those of other seasons. This is attributed to the fact that the BC emissions from biomass burning

are 17.26 Gg in the spring over Northeast China, which is significantly higher than the range of 1.02 to 3.32 Gg that is emitted in the other seasons. Additionally, the BC emitted by biomass burning in Southeast Asia during the spring is transported to south China under the influence of the southwest monsoon, which also causes the BC DREs at TOA and ATM to be higher in the spring than in the other seasons [60–62]. The maximum value of the seasonal mean BC DRE at SUR is −4.09 W m^{-2} in the summer, while the other seasonal mean values range from −3.09 to −3.98 W m^{-2}. Compared with the other seasons, the solar zenith angle is the highest in the summer, and the solar radiation is the strongest.

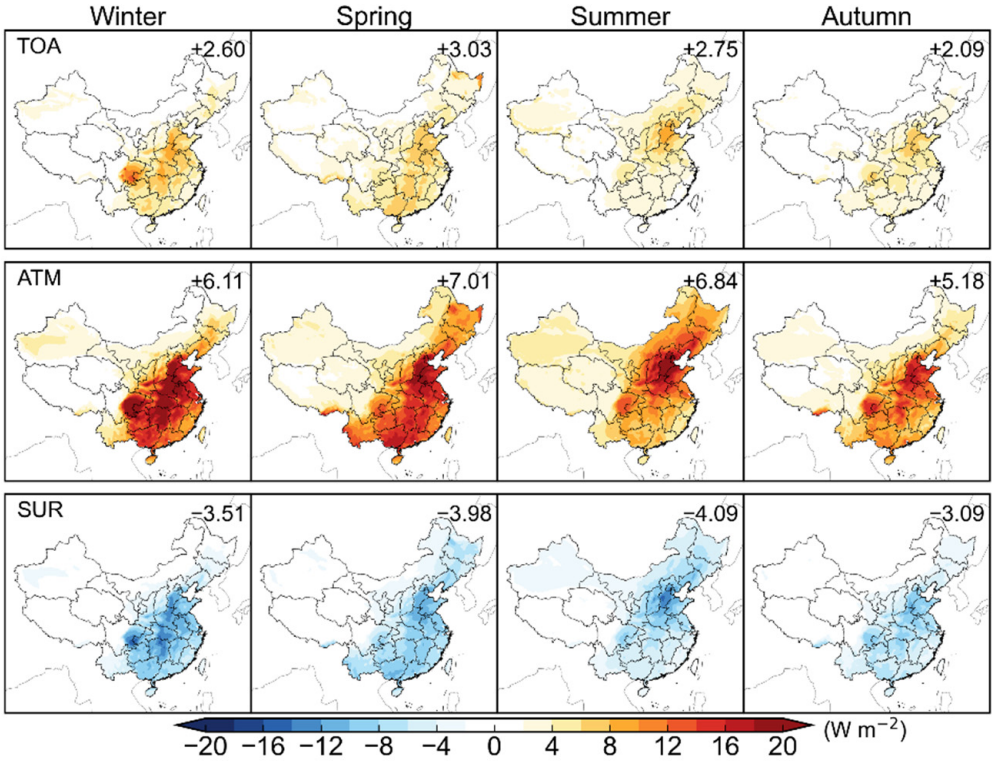

Figure 4. The spatial distributions of the seasonal mean BC clear-sky shortwave direct radiative effects (DREs) at the top-of-atmosphere (TOA), in the atmosphere (ATM) and at the surface (SUR) over China. The mean values averaged over China are shown in the upper right corner.

3.3. Impacts of Black Carbon on Photolysis Rates

The light absorption of BC reduces the actinic flux reaching the surface, thereby reducing the photolysis rates. J[O^1D] and J[HCHO] are critical drivers for the formation of the OH radical in the troposphere [63]. The photolysis of NO_2 leads to the formation of NO, which is a key precursor for O_3. Figure 5 displays the relative changes in the simulated seasonal mean photolysis rates (J[O^1D], J[NO_2] and J[HCHO]) over China after turning off BC absorption. The reductions in the annual mean J[O^1D], J[NO_2] and J[HCHO] are 4.79%, 4.03% and 4.82%, respectively. The relative change of J[O^1D] is stronger in the winter (−6.18%) and weaker in the summer (−4.06%). The spatial distributions of the relative changes in the seasonal mean J[NO_2] and J[HCHO] are similar to those of J[O^1D], with BC light absorption resulting in relative changes of −3.47% to −5.17% and −4.15% to −6.15% in J[NO_2] and J[HCHO], respectively.

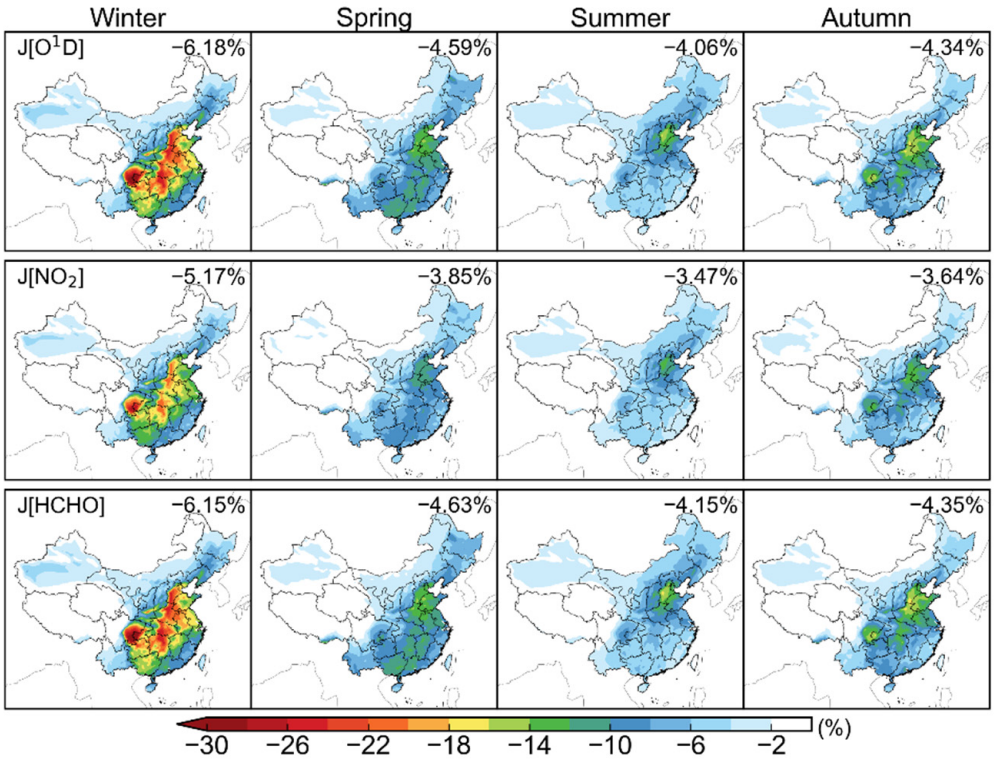

Figure 5. The spatial distributions of the relative changes in the seasonal mean surface photolysis rates (J[O^1D], J[NO_2] and J[HCHO]) after turning off BC absorption. The relative changes averaged over China are shown in the upper right corner.

3.4. Impacts of Black Carbon on Free Radicals

The OH radical is formed through a series of photochemical reactions (e.g., photolysis of O_3 and HCHO), which can be simultaneously converted into the hydroperoxyl (HO_2) radical by reacting with VOCs [64,65]. HO_x radicals are important atmospheric oxidants in the lower atmosphere and represent the atmospheric oxidizing capacity. Figure 6 shows the spatial distributions of the relative changes in the seasonal mean surface HO_x (OH and HO_2) radicals over China in the different seasons after turning off BC absorption. It was found that BC reduces the OH radical by 6.82%, 5.50%, 4.27% and 5.11% in the winter, spring, summer and autumn, respectively. In the winter, the effect of BC on the OH radical is higher than those in the other seasons, which is attributed to the higher anthropogenic emission of BC in the winter [38]. Similar to the OH radical, the relative change in surface HO_2 radicals in the winter is −4.40%, which is higher than those in other seasons (−2.14% to −3.87%). Different from the relative changes in HO_x radicals, the highest absolute changes in the seasonal means for OH and HO_2 radicals are found in the summer, with the values reaching -1.39×10^5 and -0.59×10^7 molec cm^{-3}, respectively (Figure 7). This is due to the stronger solar radiation in the summer, despite higher BC emission occurring during the winter season. In the NCP, the changes in the seasonal mean values of OH (HO_2) radicals range from -4.98×10^5 to -0.05×10^5 molec cm^{-3} (-2.0×10^7 to -0.001×10^7 molec cm^{-3}), with the values being significantly higher in the summer than in the other seasons. These results are generally consistent with the conclusions in previous studies that the concentrations of OH precursors (O_3 and formaldehyde) in the summer are higher than those in other seasons in eastern China [66,67]. In addition, we have noticed that the BC generated by wildfires in Southeast Asia results in a remarkable reduction in HO_x radicals in southern China in the spring.

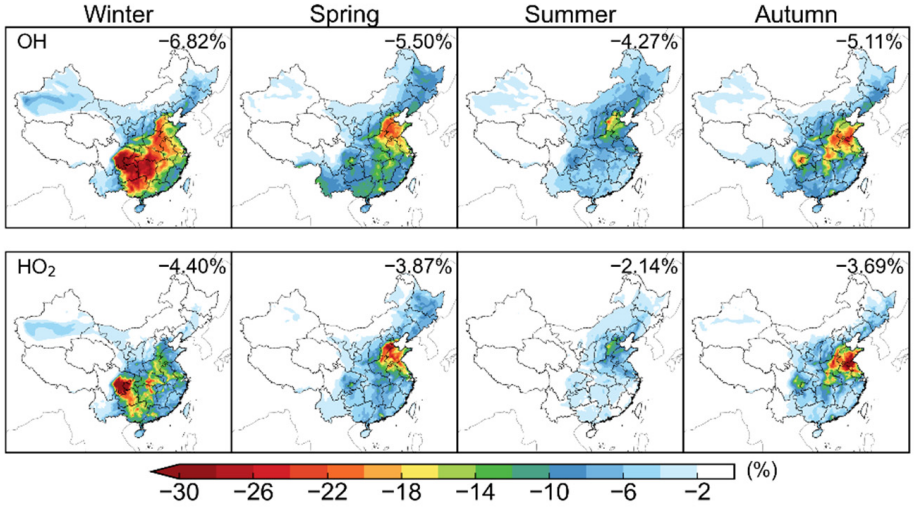

Figure 6. The spatial distributions for the relative changes in the seasonal mean surface HO_x (OH and HO_2) radicals after turning off BC absorption. The relative changes averaged over China are shown in the upper right corner.

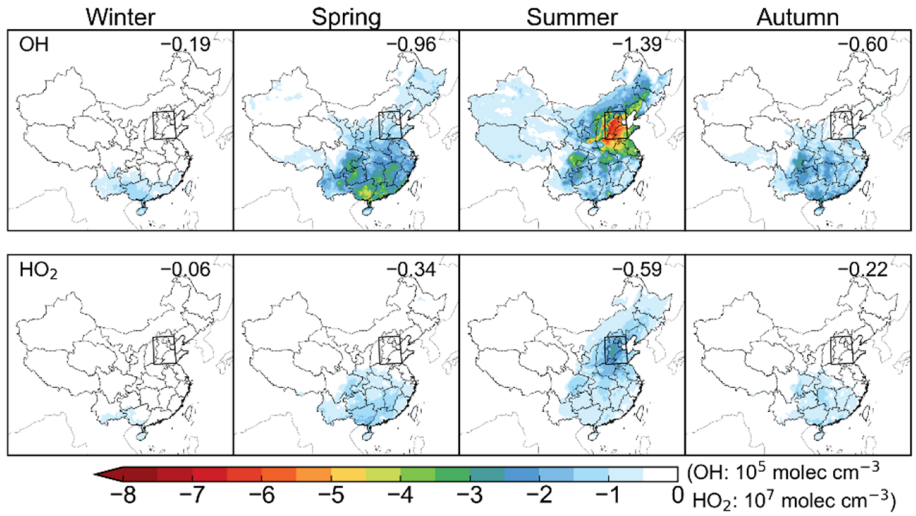

Figure 7. Same as Figure 6, but for absolute changes. Black rectangle indicates the North China Plain (NCP) region.

3.5. Impacts of Black Carbon on Ozone

O_3 is not only a pollutant in the troposphere, but it is also an important oxidant. The BC-induced reduction in photolysis rates slows down the photochemical reactions, leading to a decrease in O_3 concentrations over China. As shown in Figure 8, the seasonal mean surface O_3 concentration over China decreases by 0.31 ppb (2.37%), 0.59 ppb (1.60%), 0.26 ppb (0.47%) and 0.54 ppb (1.90%) in the winter, spring, summer and autumn, respectively. Qu et al. [68] have suggested that aerosol direct radiative effects (including scattering and absorbing) reduce the average annual O_3 concentration by 2.01 ppb (6.2%) in China. In the winter, the most noticeable reductions in O_3 concentration are concentrated in southwest China, where the basin topography facilitates the accumulation and transport of pollutants along the edge of plateau [69]. In the spring and autumn, the seasonal mean O_3 concentrations decrease by 0.59 ppb (1.60%) and 0.54 ppb (1.90%) over China, and these values are higher than those in the winter and summer. It is notable that the concentration of the O_3 reduction in the NCP region exhibits distinct seasonal variations, with a maximum value of 1.79 ppb (3.56%) in the summer, a minimum value of 0.24 ppb (3.91%) in the winter, and 1.32 (5.68%) and 0.88 ppb (6.72%) in the spring and autumn, respectively. A previous

study suggested that aerosol–photolysis interactions resulted in a reduction in the autumn O_3 concentration, ranging from 8.2 to 10.6 ppb (17.7% to 19.4%) in Beijing, Tianjin and Shijiazhuang, respectively [70]. Li et al. [23] estimated that BC caused a decrease in the regional average surface O_3 concentration by 2.0 ppb (4.4%) through a case study over the NCP in October. Compared to other factors that affect O_3 concentration, the uptake of HO_2 by aerosols led to a decrease in the average surface-layer O_3 concentration of 1 to 6 ppb over China [71]. Furthermore, in 2012, when NO_x emissions were decreased by 30%, the average surface O_3 concentrations in the NCP, YRD and PRD regions increased by 7.4%, 3.0% and 8.3% respectively. In contrast, when VOC emissions were reduced by 30%, the average O_3 concentrations in the NCP, YRD and PRD regions declined by 10.8%, 9.6% and 12.0% respectively [72]. There are obvious seasonal differences in the changes between the NCP region and southern China (south of the Yangtze River). In the NCP, the strong solar radiation in the summer and the massive production of O_3 precursors (e.g., isoprene) by vegetation contribute to higher O_3 concentrations [73,74]. In contrast, in southern China, the summer monsoon increases both cloud cover and precipitation, which suppresses the photochemical reactions leading to the formation of O_3 [75].

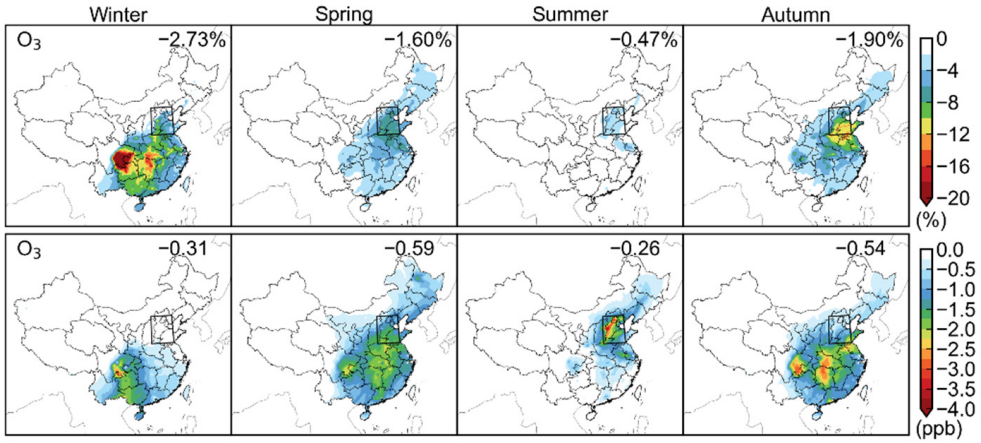

Figure 8. The spatial distributions for the relative changes (**first row**) and absolute changes (**second row**) in the seasonal mean surface O_3 concentration after turning off BC absorption. The mean values averaged over China are shown in the upper right corner. The black rectangle indicates the North China Plain (NCP) region.

4. Conclusions

In this study, we investigated the impacts of BC on the direct radiative effects (DREs) and photochemistry over China by utilizing the WRF-Chem model. The simulation results show that the seasonal mean BC concentrations at the surface over China ranges between 0.19 and 0.70 μg m^{-3}. Notably, the surface BC concentration in the NCP exceeds 3.0 μg m^{-3} in the winter and ranges between 0.57 and 1.97 μg m^{-3} in the other seasons. Corresponding to the variations of BC concentrations, the seasonal mean values of AAOD are within the range of 0.010 to 0.015 in China. The seasonal mean values of the clear-sky shortwave DREs of BC at the TOA over China are +2.60, +3.03, +2.75 and +2.09 W m^{-2} in the winter, spring, summer and autumn, respectively.

By absorbing solar radiation, BC reduces the actinic flux reaching the surface, which further leads to a decrease in the photolysis rate. The reductions in the annual mean J[O^1D], J[NO_2] and J[HCHO] are 4.79%, 4.03% and 4.82%, respectively. The formation of OH radicals in the troposphere is dependent on photochemical reactions. Similar to the seasonal variations of J[O^1D] and J[HCHO], OH and HO_2 radicals decrease by 6.82% in the winter, with these values being higher than those in the other seasons (between 4.27% and 5.50%). Similarly, BC reduces the concentrations of surface HO_2 radicals and O_3 over China by 4.40% and 2.73% in the winter, respectively. Unlike the relative change, the absolute changes of surface OH and HO_2 radicals are –1.39 × 10^5 and –0.59 × 10^7

molec cm^{-3} over China in the summer, with these values being higher than those in the other seasons. However, the reductions in the surface O_3 concentrations in China are more obvious in the spring (–0.59 ppb) and autumn (–0.54 ppb). In the summer, the reductions in the regional mean surface O_3, HO and HO_2 radicals in the NCP are 4.98×10^5 molec cm^{-3}, 2.0×10^7 molec cm^{-3} and 1.79 ppb, respectively, which are significantly higher values than those in other regions of China. In the NCP, near-surface photochemistry is more affected by BC in the summer than in winter, while the impact of BC is higher in the spring and autumn in southern China (i.e., regions south of the Yangtze River). Therefore, BC absorption results in reduced photolysis rates, thereby inhibiting the formation of atmospheric oxidants (HO_x radicals and O_3) and reducing the atmospheric oxidative capacity.

Atmospheric oxidative capacity influences the production of secondary pollutants, such as O_3 and secondary components in aerosols. When implementing emission control strategies, governments need to comprehensively take into account the reduction in $PM_{2.5}$ and gas precursor emissions and avoid increasing atmospheric oxidative capacity, which would produce more secondary pollutants. Our study evaluates the impacts of BC on photochemistry in different seasons. Additionally, it also provides a certain reference for the variation of atmospheric oxidants resulting from the reduction in BC emissions in the future.

There are still some uncertainties in our simulations, which need to be further improved in future studies. First, the mixing state of the aerosols is assumed to be a core-shell morphology in the simulation, while it is more complex in the real atmosphere and would significantly affect the optical properties of BC. Additionally, the aging process of BC is ignored in the model simulation, which thereby brings bias to the optical properties of simulated BC.

Author Contributions: Conceptualization, W.D. and M.X.; methodology, W.D.; software, W.D. and K.C.; validation, W.D., M.X. and X.H.; formal analysis, W.D.; investigation, W.D. and K.C.; resources, M.X.; data curation, M.X.; writing—original draft preparation, W.D.; writing—review and editing, W.D. and X.H.; visualization, W.D.; supervision, M.X.; project administration, M.X.; funding acquisition, M.X. All authors have read and agreed to the published version of the manuscript.

Funding: This work was supported by the National Natural Science Foundation of China (42177211).

Institutional Review Board Statement: Not applicable.

Informed Consent Statement: Not applicable.

Data Availability Statement: The datasets generated and analyzed during the current study are not publicly available but are available from the corresponding author on reasonable request.

Conflicts of Interest: The authors declare no conflicts of interest.

References

1. Bond, T.C.; Doherty, S.J.; Fahey, D.W.; Forster, P.M.; Berntsen, T.; DeAngelo, B.J.; Flanner, M.G.; Ghan, S.; Kärcher, B.; Koch, D.; et al. Bounding the role of black carbon in the climate system: A scientific assessment. *J. Geophys. Res. Atmos.* **2013**, *118*, 5380–5552. [CrossRef]
2. Wang, R.; Balkanski, Y.; Boucher, O.; Ciais, P.; Schuster, G.L.; Chevallier, F.; Samset, B.H.; Liu, J.; Piao, S.; Valari, M.; et al. Estimation of global black carbon direct radiative forcing and its uncertainty constrained by observations. *J. Geophys. Res. Atmos.* **2016**, *121*, 5948–5971. [CrossRef]
3. Wang, Q.; Jacob, D.J.; Spackman, J.R.; Perring, A.E.; Schwarz, J.P.; Moteki, N.; Marais, E.A.; Ge, C.; Wang, J.; Barrett, S.R.H. Global budget and radiative forcing of black carbon aerosol: Constraints from pole-to-pole (HIPPO) observations across the Pacific. *J. Geophys. Res. Atmos.* **2014**, *119*, 195–206. [CrossRef]
4. Zhang, A.; Wang, Y.; Zhang, Y.; Weber, R.J.; Song, Y.; Ke, Z.; Zou, Y. Modeling the global radiative effect of brown carbon: A potentially larger heating source in the tropical free troposphere than black carbon. *Atmos. Chem. Phys.* **2020**, *20*, 1901–1920. [CrossRef]
5. Huang, X.; Song, Y.; Zhao, C.; Cai, X.; Zhang, H.; Zhu, T. Direct Radiative Effect by Multicomponent Aerosol over China. *J. Clim.* **2015**, *28*, 3472–3495. [CrossRef]
6. Gao, Y.; Zhao, C.; Liu, X.; Zhang, M.; Leung, L.R. WRF-Chem simulations of aerosols and anthropogenic aerosol radiative forcing in East Asia. *Atmos. Environ.* **2014**, *92*, 250–266. [CrossRef]

7. Yang, Y.; Wang, H.; Smith, S.J.; Ma, P.L.; Rasch, P.J. Source attribution of black carbon and its direct radiative forcing in China. *Atmos. Chem. Phys.* **2017**, *17*, 4319–4336. [CrossRef]
8. Li, K.; Liao, H.; Mao, Y.; Ridley, D.A. Source sector and region contributions to concentration and direct radiative forcing of black carbon in China. *Atmos. Environ.* **2016**, *124*, 351–366. [CrossRef]
9. Shetter, R.E.; Cantrell, C.A.; Lantz, K.O.; Flocke, S.J.; Orlando, J.J.; Tyndall, G.S.; Gilpin, T.M.; Fischer, C.A.; Madronich, S.; Calvert, J.G.; et al. Actinometric and radiometric measurement and modeling of the photolysis rate coefficient of ozone to O(1 D) during Mauna Loa Observatory Photochemistry Experiment 2. *J. Geophys. Res. Atmos.* **1996**, *101*, 14631–14642. [CrossRef]
10. Lelieveld, J.; Dentener, F.J. What controls tropospheric ozone? *J. Geophys. Res. Atmos.* **2000**, *105*, 3531–3551. [CrossRef]
11. Zhang, K.; Duan, Y.; Huo, J.; Huang, L.; Wang, Y.; Fu, Q.; Wang, Y.; Li, L. Formation mechanism of HCHO pollution in the suburban Yangtze River Delta region, China: A box model study and policy implementations. *Atmos. Environ.* **2021**, *267*, 118755. [CrossRef]
12. Liu, T.; Hong, Y.; Li, M.; Xu, L.; Chen, J.; Bian, Y.; Yang, C.; Dan, Y.; Zhang, Y.; Xue, L.; et al. Atmospheric oxidation capacity and ozone pollution mechanism in a coastal city of southeastern China: Analysis of a typical photochemical episode by an observation-based model. *Atmos. Chem. Phys.* **2022**, *22*, 2173–2190. [CrossRef]
13. Yang, H.; Levy, H., II. Sensitivity of photodissociation rate coefficients and O_3 photochemical tendencies to aerosols and clouds. *J. Geophys. Res. Atmos.* **2004**, *109*. [CrossRef]
14. Tie, X.; Madronich, S.; Walters, S.; Edwards, D.P.; Ginoux, P.; Mahowald, N.; Zhang, R.; Lou, C.; Brasseur, G. Assessment of the global impact of aerosols on tropospheric oxidants. *J. Geophys. Res. Atmos.* **2005**, *110*. [CrossRef]
15. Tian, R.; Ma, X.; Jia, H.; Yu, F.; Sha, T.; Zan, Y. Aerosol radiative effects on tropospheric photochemistry with GEOS-Chem simulations. *Atmos. Environ.* **2019**, *208*, 82–94. [CrossRef]
16. Liao, H.; Yung, Y.L.; Seinfeld, J.H. Effects of aerosols on tropospheric photolysis rates in clear and cloudy atmospheres. *J. Geophys. Res. Atmos.* **1999**, *104*, 23697–23707. [CrossRef]
17. Li, G.; Zhang, R.; Fan, J.; Tie, X. Impacts of black carbon aerosol on photolysis and ozone. *J. Geophys. Res. Atmos.* **2005**, *110*. [CrossRef]
18. Real, E.; Sartelet, K. Modeling of photolysis rates over Europe: Impact on chemical gaseous species and aerosols. *Atmos. Chem. Phys.* **2011**, *11*, 1711–1727. [CrossRef]
19. Martin, R.V.; Jacob, D.J.; Yantosca, R.M.; Chin, M.; Ginoux, P. Global and regional decreases in tropospheric oxidants from photochemical effects of aerosols. *J. Geophys. Res. Atmos.* **2003**, *108*. [CrossRef]
20. Gao, J.; Li, Y.; Xie, Z.; Wang, L.; Hu, B.; Bao, F. Which aerosol type dominate the impact of aerosols on ozone via changing photolysis rates? *Sci. Total Environ.* **2023**, *854*, 158580. [CrossRef]
21. Chen, H.; Zhuang, B.; Liu, J.; Zhou, Y.; Hu, Y.; Chen, Y.; Gao, Y.; Wei, W.; Lin, H.; Li, S.; et al. Absorbing Aerosol Optical Properties and Radiative Effects on Near-Surface Photochemistry in East Asia. *Remote Sens.* **2023**, *15*, 2779. [CrossRef]
22. Gao, J.; Zhu, B.; Xiao, H.; Kang, H.; Pan, C.; Wang, D.; Wang, H. Effects of black carbon and boundary layer interaction on surface ozone in Nanjing, China. *Atmos. Chem. Phys.* **2018**, *18*, 7081–7094. [CrossRef]
23. Li, J.; Li, Y. Ozone deterioration over North China plain caused by light absorption of black carbon and organic carbon. *Atmos. Environ.* **2023**, *313*, 120048. [CrossRef]
24. Grell, G.A.; Peckham, S.E.; Schmitz, R.; McKeen, S.A.; Frost, G.; Skamarock, W.C.; Eder, B. Fully coupled "online" chemistry within the WRF model. *Atmos. Environ.* **2005**, *39*, 6957–6975. [CrossRef]
25. Emmons, L.K.; Walters, S.; Hess, P.G.; Lamarque, J.F.; Pfister, G.G.; Fillmore, D.; Granier, C.; Guenther, A.; Kinnison, D.; Laepple, T.; et al. Description and evaluation of the Model for Ozone and Related chemical Tracers, version 4 (MOZART-4). *Geosci. Model Dev.* **2010**, *3*, 43–67. [CrossRef]
26. Zaveri, R.A.; Easter, R.C.; Fast, J.D.; Peters, L.K. Model for Simulating Aerosol Interactions and Chemistry (MOSAIC). *J. Geophys. Res. Atmos.* **2008**, *113*. [CrossRef]
27. Zhu, Y.; Wang, Q.; Yang, X.; Yang, N.; Wang, X. Modeling Investigation of Brown Carbon Aerosol and Its Light Absorption in China. *Atmosphere* **2021**, *12*, 892. [CrossRef]
28. Yang, L.; Mao, Y.; Liao, H.; Xie, M.; Zhang, Y. Direct radiative forcing of light-absorbing carbonaceous aerosols in China. *Atmos. Res.* **2024**, *304*, 107396. [CrossRef]
29. Bond, T.C.; Bergstrom, R.W. Light Absorption by Carbonaceous Particles: An Investigative Review. *Aerosol Sci. Technol.* **2006**, *40*, 27–67. [CrossRef]
30. Morrison, H.; Curry, J.A.; Khvorostyanov, V.I. A New Double-Moment Microphysics Parameterization for Application in Cloud and Climate Models. Part I: Description. *J. Atmos. Sci.* **2005**, *62*, 1665–1677. [CrossRef]
31. Grell, G.A. Prognostic Evaluation of Assumptions Used by Cumulus Parameterizations. *Mon. Weather Rev.* **1993**, *121*, 764–787. [CrossRef]
32. Iacono, M.J.; Delamere, J.S.; Mlawer, E.J.; Shephard, M.W.; Clough, S.A.; Collins, W.D. Radiative forcing by long-lived greenhouse gases: Calculations with the AER radiative transfer models. *J. Geophys. Res. Atmos.* **2008**, *113*. [CrossRef]
33. Chen, F.; Dudhia, J. Coupling an Advanced Land Surface–Hydrology Model with the Penn State–NCAR MM5 Modeling System. Part I: Model Implementation and Sensitivity. *Mon. Weather Rev.* **2001**, *129*, 569–585. [CrossRef]
34. Hong, S.-Y.; Noh, Y.; Dudhia, J. A New Vertical Diffusion Package with an Explicit Treatment of Entrainment Processes. *Mon. Weather Rev.* **2006**, *134*, 2318–2341. [CrossRef]

35. Hersbach, H.; Bell, B.; Berrisford, P.; Hirahara, S.; Horányi, A.; Muñoz-Sabater, J.; Nicolas, J.; Peubey, C.; Radu, R.; Schepers, D.; et al. The ERA5 global reanalysis. *Q. J. R. Meteorol. Soc.* **2020**, *146*, 1999–2049. [CrossRef]
36. Li, M.; Liu, H.; Geng, G.; Hong, C.; Liu, F.; Song, Y.; Tong, D.; Zheng, B.; Cui, H.; Man, H.; et al. Anthropogenic emission inventories in China: A review. *Natl. Sci. Rev.* **2017**, *4*, 834–866. [CrossRef]
37. Li, M.; Zhang, Q.; Kurokawa, J.-i.; Woo, J.-H.; He, K.; Lu, Z.; Ohara, T.; Song, Y.; Streets, D.G.; Carmichael, G.R.; et al. MIX: A mosaic Asian anthropogenic emission inventory under the international collaboration framework of the MICS-Asia and HTAP. *Atmos. Chem. Phys.* **2017**, *17*, 935–963. [CrossRef]
38. Zheng, B.; Tong, D.; Li, M.; Liu, F.; Hong, C.; Geng, G.; Li, H.; Li, X.; Peng, L.; Qi, J.; et al. Trends in China's anthropogenic emissions since 2010 as the consequence of clean air actions. *Atmos. Chem. Phys.* **2018**, *18*, 14095–14111. [CrossRef]
39. Guenther, A.; Karl, T.; Harley, P.; Wiedinmyer, C.; Palmer, P.I.; Geron, C. Estimates of global terrestrial isoprene emissions using MEGAN (Model of Emissions of Gases and Aerosols from Nature). *Atmos. Chem. Phys.* **2006**, *6*, 3181–3210. [CrossRef]
40. Giglio, L.; Randerson, J.T.; van der Werf, G.R. Analysis of daily, monthly, and annual burned area using the fourth-generation global fire emissions database (GFED4). *J. Geophys. Res. Biogeosciences* **2013**, *118*, 317–328. [CrossRef]
41. Randerson, J.T.; Chen, Y.; van der Werf, G.R.; Rogers, B.M.; Morton, D.C. Global burned area and biomass burning emissions from small fires. *J. Geophys. Res. Biogeosci.* **2012**, *117*. [CrossRef]
42. Lamarque, J.F.; Emmons, L.K.; Hess, P.G.; Kinnison, D.E.; Tilmes, S.; Vitt, F.; Heald, C.L.; Holland, E.A.; Lauritzen, P.H.; Neu, J.; et al. CAM-chem: Description and evaluation of interactive atmospheric chemistry in the Community Earth System Model. *Geosci. Model Dev.* **2012**, *5*, 369–411. [CrossRef]
43. Emmons, L.K.; Schwantes, R.H.; Orlando, J.J.; Tyndall, G.; Kinnison, D.; Lamarque, J.-F.; Marsh, D.; Mills, M.J.; Tilmes, S.; Bardeen, C.; et al. The Chemistry Mechanism in the Community Earth System Model Version 2 (CESM2). *J. Adv. Model. Earth Syst.* **2020**, *12*, e2019MS001882. [CrossRef]
44. Holbena, B.N.; Eckb, T.; Slutskerc, I.; Smirnovb, A.; Sinyukc, A.; Schaferc, J.; Gilesc, D.; Dubovikd, O. AERONET's Version 2.0 quality assurance criteria. In *Remote Sensing of the Atmosphere and Clouds*; SPIE: St Bellingham, WA, USA, 2006.
45. Sun, J.; Qin, M.; Xie, X.; Fu, W.; Qin, Y.; Sheng, L.; Li, L.; Li, J.; Sulaymon, I.D.; Jiang, L.; et al. Seasonal modeling analysis of nitrate formation pathways in Yangtze River Delta region, China. *Atmos. Chem. Phys.* **2022**, *22*, 12629–12646. [CrossRef]
46. Yang, H.; Chen, L.; Liao, H.; Zhu, J.; Wang, W.; Li, X. Weakened aerosol–radiation interaction exacerbating ozone pollution in eastern China since China's clean air actions. *Atmos. Chem. Phys.* **2024**, *24*, 4001–4015. [CrossRef]
47. Qu, Y.; Wang, T.; Yuan, C.; Wu, H.; Gao, L.; Huang, C.; Li, Y.; Li, M.; Xie, M. The underlying mechanisms of PM2.5 and O_3 synergistic pollution in East China: Photochemical and heterogeneous interactions. *Sci. Total Environ.* **2023**, *873*, 162434. [CrossRef]
48. Ping, L.; Wang, Y.; Lu, Y.; Lee, L.-C.; Liang, C. Tracing the sources of PM2.5-related health burden in China. *Environ. Pollut.* **2023**, *327*, 121544. [CrossRef]
49. Yang, H.; Chen, L.; Liao, H.; Zhu, J.; Wang, W.; Li, X. Impacts of aerosol–photolysis interaction and aerosol–radiation feedback on surface-layer ozone in North China during multi-pollutant air pollution episodes. *Atmos. Chem. Phys.* **2022**, *22*, 4101–4116. [CrossRef]
50. Yang, H.; Chen, L.; Liao, H.; Zhu, J.; Wang, W.; Li, X. Impact of physical parameterizations on wind simulation with WRF V3.9.1.1 under stable conditions at planetary boundary layer gray-zone resolution: A case study over the coastal regions of North China. *Geosci. Model Dev.* **2022**, *15*, 8111–8134.
51. Hu, J.; Chen, J.; Ying, Q.; Zhang, H. One-year simulation of ozone and particulate matter in China using WRF/CMAQ modeling system. *Atmos. Chem. Phys.* **2016**, *16*, 10333–10350. [CrossRef]
52. Zhang, C.; He, J.; Lai, X.; Liu, Y.; Che, H.; Gong, S. The Impact of the Variation in Weather and Season on WRF Dynamical Downscaling in the Pearl River Delta Region. *Atmosphere* **2021**, *12*, 409. [CrossRef]
53. Wang, Y.; Cao, L.; Zhang, T.; Kong, H. Simulations of Summertime Ozone and PM2.5 Pollution in Fenwei Plain (FWP) Using the WRF-Chem Model. *Atmosphere* **2023**, *14*, 292. [CrossRef]
54. Yang, J.; Zhao, Y. Performance and application of air quality models on ozone simulation in China—A review. *Atmos. Environ.* **2023**, *293*, 119446. [CrossRef]
55. Miao, R.; Chen, Q.; Zheng, Y.; Cheng, X.; Sun, Y.; Palmer, P.I.; Shrivastava, M.; Guo, J.; Zhang, Q.; Liu, Y.; et al. Model bias in simulating major chemical components of PM2.5 in China. *Atmos. Chem. Phys.* **2020**, *20*, 12265–12284. [CrossRef]
56. Xu, Y.; Xue, W.; Lei, Y.; Zhao, Y.; Cheng, S.; Ren, Z.; Huang, Q. Impact of Meteorological Conditions on PM2.5 Pollution in China during Winter. *Atmosphere* **2018**, *9*, 429. [CrossRef]
57. Li, J.; Liao, H.; Hu, J.; Li, N. Severe particulate pollution days in China during 2013–2018 and the associated typical weather patterns in Beijing-Tianjin-Hebei and the Yangtze River Delta regions. *Environ. Pollut.* **2019**, *248*, 74–81. [CrossRef]
58. Zhang, X.; Zhou, L.; Zhang, X.; Luo, Y.; Sun, L. A Case Study on the Impact of East Asian Summer Monsoon on Surface O_3 in China. *Atmosphere* **2023**, *14*, 768. [CrossRef]
59. Cui, F.; Pei, S.; Chen, M.; Ma, Y. Seasonal variation and source analyses of aerosol optical properties in Nanjing, China. *Atmos. Pollut. Res.* **2021**, *12*, 101117. [CrossRef]
60. Zhu, J.; Yue, X.; Zhou, H.; Che, H.; Xia, X.; Wang, J.; Zhao, T.; Tian, C.; Liao, H. The multi-year contribution of Indo-China peninsula fire emissions to aerosol radiation forcing in southern China during 2013–2019. *Sci. Total Environ.* **2024**, *927*, 172337. [CrossRef]

61. Zhu, J.; Xia, X.; Wang, J.; Zhang, J.; Wiedinmyer, C.; Fisher, J.A.; Keller, C.A. Impact of Southeast Asian smoke on aerosol properties in Southwest China: First comparison of model simulations with satellite and ground observations. *J. Geophys. Res. Atmos.* **2017**, *122*, 3904–3919. [CrossRef]
62. Zhang, L.; Ding, S.; Qian, W.; Zhao, A.; Zhao, S.; Yang, Y.; Weng, G.; Tao, M.; Chen, H.; Zhao, S.; et al. The Impact of Long-Range Transport of Biomass Burning Emissions in Southeast Asia on Southern China. *Atmosphere* **2022**, *13*, 1029. [CrossRef]
63. Mellouki, A.; Wallington, T.J.; Chen, J. Atmospheric Chemistry of Oxygenated Volatile Organic Compounds: Impacts on Air Quality and Climate. *Chem. Rev.* **2015**, *115*, 3984–4014. [CrossRef] [PubMed]
64. Lu, K.; Guo, S.; Tan, Z.; Wang, H.; Shang, D.; Liu, Y.; Li, X.; Wu, Z.; Hu, M.; Zhang, Y. Exploring atmospheric free-radical chemistry in China: The self-cleansing capacity and the formation of secondary air pollution. *Natl. Sci. Rev.* **2018**, *6*, 579–594. [CrossRef] [PubMed]
65. Ma, X.; Tan, Z.; Lu, K.; Yang, X.; Liu, Y.; Li, S.; Li, X.; Chen, S.; Novelli, A.; Cho, C.; et al. Winter photochemistry in Beijing: Observation and model simulation of OH and HO2 radicals at an urban site. *Sci. Total Environ.* **2019**, *685*, 85–95. [CrossRef] [PubMed]
66. Li, K.; Jacob, D.J.; Shen, L.; Lu, X.; De Smedt, I.; Liao, H. Increases in surface ozone pollution in China from 2013 to 2019: Anthropogenic and meteorological influences. *Atmos. Chem. Phys.* **2020**, *20*, 11423–11433. [CrossRef]
67. Sun, Y.; Yin, H.; Liu, C.; Zhang, L.; Cheng, Y.; Palm, M.; Notholt, J.; Lu, X.; Vigouroux, C.; Zheng, B.; et al. Mapping the drivers of formaldehyde (HCHO) variability from 2015 to 2019 over eastern China: Insights from Fourier transform infrared observation and GEOS-Chem model simulation. *Atmos. Chem. Phys.* **2021**, *21*, 6365–6387. [CrossRef]
68. Qu, Y.; Voulgarakis, A.; Wang, T.; Kasoar, M.; Wells, C.; Yuan, C.; Varma, S.; Mansfield, L. A study of the effect of aerosols on surface ozone through meteorology feedbacks over China. *Atmos. Chem. Phys.* **2021**, *21*, 5705–5718. [CrossRef]
69. Shen, L.; Liu, J.; Zhao, T.; Xu, X.; Han, H.; Wang, H.; Shu, Z. Atmospheric transport drives regional interactions of ozone pollution in China. *Sci. Total Environ.* **2022**, *830*, 154634. [CrossRef]
70. Gao, J.; Li, Y.; Zhu, B.; Hu, B.; Wang, L.; Bao, F. What have we missed when studying the impact of aerosols on surface ozone via changing photolysis rates? *Atmos. Chem. Phys.* **2020**, *20*, 10831–10844. [CrossRef]
71. Lou, S.; Liao, H.; Zhu, B. Impacts of aerosols on surface-layer ozone concentrations in China through heterogeneous reactions and changes in photolysis rates. *Atmos. Environ.* **2014**, *85*, 123–138. [CrossRef]
72. Wang, N.; Lyu, X.; Deng, X.; Huang, X.; Jiang, F.; Ding, A. Aggravating O_3 pollution due to NOx emission control in eastern China. *Sci. Total Environ.* **2019**, *677*, 732–744. [CrossRef] [PubMed]
73. Wang, W.; Parrish, D.D.; Wang, S.; Bao, F.; Ni, R.; Li, X.; Yang, S.; Wang, H.; Cheng, Y.; Su, H. Long-term trend of ozone pollution in China during 2014–2020: Distinct seasonal and spatial characteristics and ozone sensitivity. *Atmos. Chem. Phys.* **2022**, *22*, 8935–8949. [CrossRef]
74. Wang, H.; Wu, Q.; Guenther, A.B.; Yang, X.; Wang, L.; Xiao, T.; Li, J.; Feng, J.; Xu, Q.; Cheng, H. A long-term estimation of biogenic volatile organic compound (BVOC) emission in China from 2001–2016: The roles of land cover change and climate variability. *Atmos. Chem. Phys.* **2021**, *21*, 4825–4848. [CrossRef]
75. Yin, C.Q.; Solmon, F.; Deng, X.J.; Zou, Y.; Deng, T.; Wang, N.; Li, F.; Mai, B.R.; Liu, L. Geographical distribution of ozone seasonality over China. *Sci. Total Environ.* **2019**, *689*, 625–633. [CrossRef] [PubMed]